Title
A high dust emissivity index β for a CO-faint galaxy in a filamentary Lyα nebula at z = 3.1

Journal
Publications of the Astronomical Society of Japan, 70(5)

ISSN
0004-6264

Authors
Kato, Yuta
Matsuda, Yuichi
Iono, Daisuke
et al.

Publication Date
2018-10-01

DOI
10.1093/pasj/psy087

Peer reviewed

doi: 10.1093/pasj/xxx000

A high dust emissivity index β for a CO-faint galaxy in a filamentary Lyα nebula at $z = 3.1$

Yuta Kato[1,2], Yuichi Matsuda[1,3], Daisuke Iono[1,3], Bunyo Hatsukade[4], Hideki Umehata[4,5], Kotaro Kohno[4,6], David M. Alexander[7], Yiping Ao[1,8], Scott C. Chapman[9], Matthew Hayes[10], Mariko Kubo[1], Bret D. Lehmer[11], Matthew A. Malkan[12], Tomonari Michiyama[1,3], Tohru Nagao[13], Tomoki Saito[14], Ichi Tanaka[15] and Yoshiaki Taniguchi[16]

[1]National Astronomical Observatory of Japan, 2-21-1 Osawa, Mitaka, Tokyo, 181-8588, Japan
[2]Department of Astronomy, Graduate School of Science, The University of Tokyo, 7-3-1 Hongo, Bunkyo-ku, Tokyo 133-0033, Japan
[3]Department of Astronomy, School of Science, The Graduate University for Advanced Studies (SOKENDAI), Osawa, Mitaka, Tokyo, 181-8588, Japan
[4]Institute of Astronomy, Graduate School of Science, The University of Tokyo, 2-21-1 Osawa, Mitaka, Tokyo 181-0015, Japan
[5]RIKEN Cluster for Pioneering Research, 2-1 Hirosawa, Wako-shi, Saitama 351-0198, Japan
[6]Research Center for the Early Universe, Graduate School of Science, The University of Tokyo, 7-3-1 Hongo, Bunkyo, Tokyo 113-0033
[7]Centre for Extragalactic Astronomy, Department of Physics, Durham University, South Road, Durham, DH1 3LE, UK
[8]Purple Mountain Observatory, Chinese Academy of Sciences, Nanjing 210034, China
[9]Department of Physics and Atmospheric Science, Dalhousie University, Halifax, NS, B3H 4R2, Canada
[10]Department of Astronomy and Oskar Klein Centre for Cosmoparticle Physics, Stockholm University, AlbaNova University Centre, SE-106 91 Stockholm, Sweden
[11]Department of Physics, University of Arkansas, 226 Physics Building, 825 West Dickson, Fayetteville, AR 72701, USA
[12]Department of Physics and Astronomy, University of California, Los Angeles, CA 90095, USA
[13]Research Center for Space and Cosmic Evolution, Ehime University, 2-5 Bunkyo-cho, Matsuyama, Ehime 790-8577
[14]Nishi-Harima Astronomical Observatory, Centre for Astronomy, University of Hyogo, 407-2 Nichigaichi, Sayo-cho, Sayo, Hyogo 679-5313, Japan
[15]Subaru Telescope, National Astronomical Observatory of Japan, 650 North AâĂŹohoku Place, Hilo, HI 96720, USA
[16]The Open University of Japan, 2-11, Wakaba, Mihama-ku, Chiba, 261-8586

*E-mail: kato.yu@nao.ac.jp, yuta.astrophysics@gmail.com

Received 14-May-2018; Accepted 17-Jul-2018

Abstract

We present CO $J = 4 - 3$ line and 3 mm dust continuum observations of a 100 kpc-scale filamentary Lyα nebula (SSA22 LAB18) at $z = 3.1$ using the Atacama Large Millimeter/submillimeter Array (ALMA). We detected the CO $J = 4 - 3$ line at a systemic

$z_{\rm CO} = 3.093 \pm 0.001$ at 11 σ from one of the ALMA continuum sources associated with the Lyα filament. We estimated the CO $J = 4-3$ luminosity of $L'_{\rm CO(4-3)} = (2.3 \pm 0.2) \times 10^9\,{\rm K\,km\,s^{-1}\,pc^2}$ for this CO source, which is one order of magnitude smaller than those of typical $z > 1$ dusty star-forming galaxies (DSFGs) of similar far-infrared luminosity $L_{\rm IR} \sim 10^{12}\,L_\odot$. We derived a molecular gas mass of $M_{\rm gas} = (4.4^{+0.9}_{-0.6}) \times 10^9\,M_\odot$ and a star-formation rate of SFR$= 270 \pm 160\,M_\odot\,{\rm yr^{-1}}$. We also estimated a gas depletion time of $\tau_{\rm dep} = 17 \pm 10\,{\rm Myr}$, being shorter than those of typical DSFGs. It is suggested that this source is in a transition phase from DSFG to a gas-poor, early-type galaxy. From ALMA to *Herschel* multi-band dust continuum observations, we measured a dust emissivity index $\beta = 2.3 \pm 0.2$, which is similar to those of local gas-poor, early-type galaxies. Such a high β can be reproduced by specific chemical compositions for interstellar dust at the submillimeter wavelengths from recent laboratory experiments. ALMA CO and multi-band dust continuum observations can constrain the evolutionary stage of high-redshift galaxies through $\tau_{\rm dep}$ and β, and thus we can investigate dust chemical compositions even in the early Universe.

Key words: submillimeter: galaxies — galaxies: starburst — galaxies: formation — galaxies: ISM — galaxies: high-redshift

1 Introduction

Lyα blobs (LABs) are extended Lyα emitting nebulae, primarily found in galaxy over-dense regions at $z \sim 1-3$ (e.g., Steidel et al. 2000; Matsuda et al. 2004; Matsuda et al. 2009; Matsuda et al. 2011; Dey et al. 2005; Prescott et al. 2008; Barger, Cowie, & Wold 2012; Valentino et al. 2016; Caminha et al. 2016; Cai et al. 2017). It has been found that some 100 kpc-scale LABs are bright in submillimeter/millimeter wavelengths, suggesting a possible connection between LABs and dusty star-forming galaxies (DSFGs, e.g.,Chapman et al. 2001; Chapman et al. 2004; Geach et al. 2005; Geach et al. 2014; Tamura et al. 2013; Yang et al. 2014; Hine et al. 2016; Alexander et al. 2016; Ao et al. 2017; Umehata et al. 2017a; Umehata et al. 2017b; Umehata et al. 2018). However, we don't know if the DSFGs in LABs differ from typical DSFGs population.

Molecular gas depletion time ($\tau_{\rm dep}$) is given by the ratio of molecular gas mass ($M_{\rm gas}$) over star-formation rate (SFR), and is useful to investigate the evolutionary stage of DSFGs (e.g., Chapman et al. 2004; Greve et al. 2005; Hodge et al. 2013; Ginolfi et al. 2017). Typically DSFGs have a $\tau_{\rm dep} \lesssim 10^8\,{\rm yr}$, while less active high-redshift star-forming galaxies have much longer timescales (e.g., Tacconi et al. 2018). Since there are very few LABs where molecular gas has been detected, it is unclear which evolutionary stage of dusty star-formation exists in LABs, and how long dusty star-formation of LABs will continue. While LABs would be the seeds of galaxy groups and experience very rapid galaxy assembly (e.g., Prescott et al. 2012; Kubo et al. 2016; Bădescu et al. 2017), it is yet to be understood what they evolve into.

For the study of the interstellar medium (ISM), the dust emissivity index (β) at submillimeter wavelengths is derived from the Rayleigh-Jeans tail of infrared (IR) spectral energy distribution (SED), which reflects the dust chemical compositions (Galliano, Galametz, & Jones 2017). The IR SED is often approximated by a modified black body model of $S_{\rm obs} = (M_{\rm d}/D_{\rm L}^2)\,\kappa_0(\nu/\nu_0)^\beta\,B_\nu(\nu_{\rm rest}, T_{\rm d})$ (Hildebrand 1983), where $M_{\rm d}$ is dust mass, $D_{\rm L}^2$ is luminosity distance, κ_0 is mass absorption coefficient at frequency ν_0, β is its variation as a function of frequency, and $B_\nu(\nu_{\rm rest}, T_{\rm d})$ is the Planck function. Different materials can produce different Îš, for instance, Crystalline Silicate have $\beta = 2.0$ and Amorphous Graphite have $\beta = 1.0$, which both change with temperature and frequency range (e.g., Jones 2002; Meny et al. 2007).

The dust emissivity index β has also been studied in relation to galaxy properties in the local Universe. Boselli et al. (2012) reports lower β in low metallicity galaxies and Cortese et al. (2014) reports higher β in local gas-poor, early-type galaxies with *Herschel*/SPIRE. While local galaxies have $\beta \sim$1.0-2.5 (e.g., Dunne et al. 2000; Smith et al. 2013; Clements et al. 2018), it has been difficult to measure β for high-redshift galaxies. The high sensitivity of the Atacama Large Millimeter/submillimeter Array (ALMA) now allows us to constrain β for high-redshift galaxies (e.g., Tadaki et al. 2017).

Our target is SSA22 LAB18 at R.A. (J2000) = 22h17m29.0s, decl. (J2000) = +00°07′50″ (Matsuda et al. 2004) in the SSA22 protocluster at $z = 3.1$ (Steidel et al. 1998). LAB18 has a Lyα luminosity of $L_{\rm Lyff} = (0.8 \pm 0.2) \times 10^{43}\,{\rm erg\ s^{-1}}$, physical size of $100 \times 30\,{\rm kpc}$, and spectroscopic redshift of $z_{\rm Lyff} = 3.104$ (Matsuda et al. 2011). LAB18 has been detected by using James Clerk Maxwell

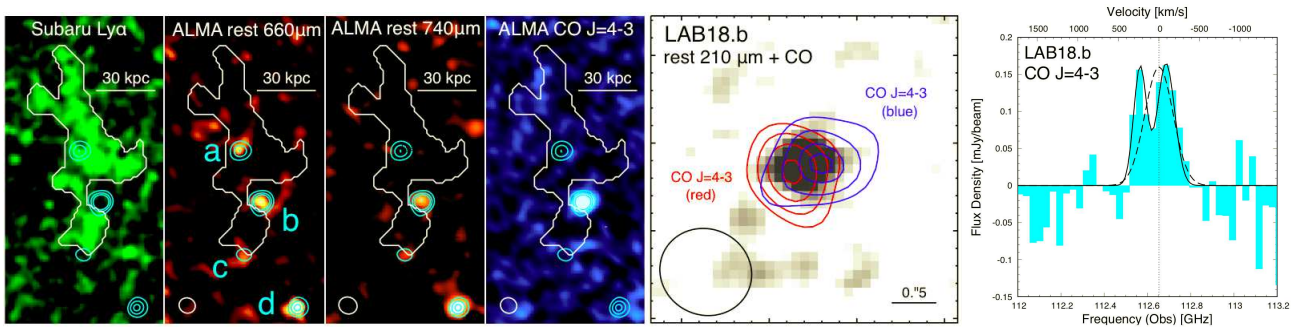

Fig. 1. *(left).* Thumbnail images of the 100 kpc-scale filamentary Lyα nebula (SSA22 LAB18) at $z = 3.1$. The image size is $10'' \times 20''$ ($\sim$80$\times$160 kpc^2). From left to right, we show the Subaru/Suprime-Cam Lyα (Matsuda et al. 2004), ALMA rest-frame 660 μm, 740 μm continuum and ALMA CO $J = 4 - 3$ (This work).White contours show the Lyα emission with a surface brightness of 1.4×10^{-18} erg s^{-1} cm^{-2} arcsec^{-2}. Cyan contours show the ALMA rest-frame 210 μm continuum (LAB18.a, b ,c ,d) possibly associated with the filamentary Lyα nebula (Ao et al. 2017, Matsuda et al. in prep). *(middle).* The red and blue components of CO $J = 4 - 3$ lines for LAB18.b, which are shown as red and blue contours overlaid the ALMA rest-frame 210 μm continuum. The Red and blue contour levels are 3, 4, 5, 6 σ and 3, 4, 5, 5.5 σ, respectively. The spatial offset between the two components is $0''.4$ or $\sim$3 kpc. The image size is $3''.5 \times 3''.5$ ($\sim$30$\times$30 kpc^2). The ellipses at the bottom-left corner represent the beam FWHM for the ALMA observations for left and right panels. *(right).* The CO $J = 4 - 3$ spectrum for LAB18.b with a velocity resolution of 80 km s^{-1}. The best-fit single and double Gaussian profiles are overlaid as dashed and solid curves, respectively.

Telescope (JCMT) (Chapman et al. 2001; Chapman et al. 2004; Geach et al. 2005; Hine et al. 2016; Ao et al. 2017) and *Chandra* (Lehmer et al. 2009; Geach et al. 2009). An X-ray detection with *Chandra* observations suggests that LAB18 likely has a rapidly growing black hole in addition to the very rapid galaxy growth. ALMA 850 μm dust continuum observations (Ao et al. 2017, Matsuda et al. in prep) identified four continuum sources (LAB18.a ,b ,c ,d) toward the asymmetric, long filamentary structure of Lyα emission of LAB18 (Figure 1 left). Since LAB18 is the brightest at 850 μm among the LABs in the SSA22 protocluster, this source is the best target to conduct CO and multi-band dust continuum observations to investigate $\tau_{\rm dep}$ and β. By combining these values, we can constrain the evolutionary stage of LABs and DSFGs. We use the following cosmological parameters: $\Omega_m = 0.315$, $\Omega_\Lambda = 0.685$, $h = 0.67$ (Planck Collaboration et al. 2014a). In this cosmology, $1''.0$ corresponds to 7.9 kpc in physical length at $z = 3.1$.

Table 1. Galaxy properties for LAB18.b at $z = 3.1$.

ID	Units	LAB18.b
RA	(J2000)	22:17:28.94
Dec	(J2000)	+00:07:47.0
$z_{\rm CO(4-3)}$	–	3.093 ± 0.001
$S_{2.7\,\rm mm}$	(μJy)	52 ± 11
$S_{3\,\rm mm}$	(μJy)	29 ± 5
$S_{\rm CO(4-3)}dv$	(Jy km s^{-1})	0.083 ± 0.006
FWHM$_{\rm CO(4-3)}$	(km s^{-1})	407 ± 142
$L'_{\rm CO(4-3)}$	(10^9 K km s^{-1} pc^2)	2.3 ± 0.2
$M^a_{\rm gas}$	($10^9\,M_\odot$)	$4.4^{+0.9}_{-0.6}$
$M^b_{\rm dust,3\,mm}$	($10^7\,M_\odot$)	4.8 ± 0.8
$\delta^c_{\rm GDR}$	–	93^{+19}_{-14}
$T^d_{\rm dust}$	(K)	31.7 ± 4.1
β^d	(–)	2.3 ± 0.2
$L^d_{\rm IR}$	($10^{12}\,L_\odot$)	2.7 ± 1.6
SFR^d	($M_\odot$ yr^{-1})	269 ± 158
$\tau_{\rm dep}$	(Myr)	17 ± 10

Notes.
[a]Gas mass with r_{41}=0.41 $\pm$ 0.07 and $\alpha = 0.8\,M_\odot$ (K km s^{-1} pc^2)$^{-1}$.
[b]Dust mass with $\beta = 2.3$, $T_{\rm d} = 31.7$ K and $\kappa_{850} = 3.2$ cm^2 g^{-1}.
[c]Gas-to-dust mass ratio.
[d]The errors come from the IR SED fitting.

2 OBSERVATIONS

We observed the LAB18 in ALMA Cycle 4 project (ID: 2016.1.01101.S; PI: Y. Kato). The ALMA Band 3 observations were carried out through 12th to 14th November 2016 with 39–41 antennas with the baseline lengths of 15–1039 m ($\sim$4–290 kλ) in the dual-polarization setup. The total on-source integration time was $\sim$5 hours. The spectral windows were set to $\sim$97–101 GHz and $\sim$109-113 GHz, which covers CO $J = 4 - 3$ line from $z_{\rm CO} = 3.08 - 3.23$. J2148+0657 and J0006–0623 were observed as flux calibrators. The bandpass and phase were calibrated with J2148+0657 and J2226+0052, respectively. The accuracy of absolute flux calibration is within 10%.

We reduced the data with the Common Astronomy Software Applications (CASA; McMullin et al. 2007) 4.7.2 package in a standard manner. From the calibrated data produced by the pipeline, we made primary beam corrected line free 3 mm and 2.7 mm continuum images with 97–101 GHz and 109–113 GHz bands, and a continuum subtracted spectral cube with a 80 km s^{-1} velocity resolution using CLEAN with natural weighting. The synthesized beam full-width at half maximum (FWHM) of 3 mm and 2.7 mm continuum images are $1''.20 \times 1''.08$ with PA=65° and $1''.05 \times 0''.98$ with PA=67°, respectively. The achieved typical synthesized beam FWHM for CO

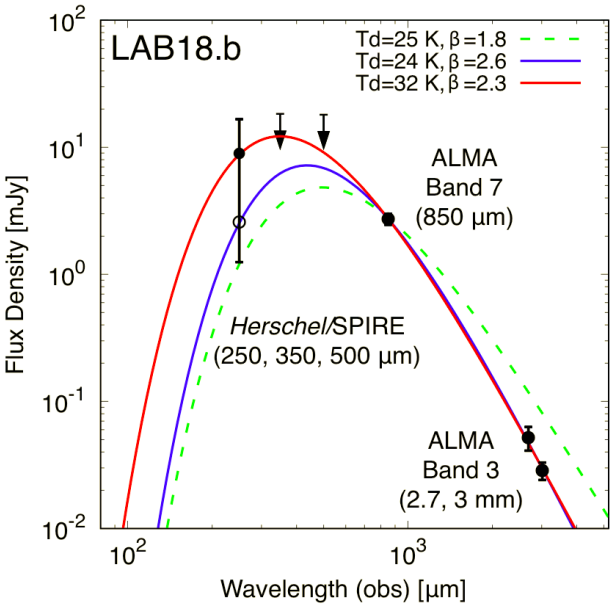

Fig. 2. The infrared (IR) spectral energy distribution (SED) for LAB18.b based on *Herschel*/SPIRE and ALMA photometry. We use a single temperature, optically thin modified black body model. The best-fit values are $T_{\rm d} = 31.7 \pm 4.1$ K, $\beta = 2.3 \pm 0.2$, and $L_{\rm IR} = (2.7 \pm 1.6) \times 10^{12}\,L_\odot$ (red solid curve). Dashed curve is for the supplementary purpose and the open circle at the SPIRE 250 μm decreases by a factor of three for its filled circle (§3.2).

spectral cube is $1\farcs07 \times 0\farcs99$ with PA=67° at 112.65 GHz. The rms noises of the 3 mm and 2.7 mm continuum images are 5.9 μJy beam^{-1} and 8.7 μJy beam^{-1}, respectively. The pixel size is set to $0\farcs1$ for all data.

3 RESULTS

3.1 CO $J = 4 - 3$ line

The CO $J = 4 - 3$ emission from LAB18.b is detected at 11 σ (peak flux to map variance on the integrated map). The derived systemic redshift is $z_{\rm CO} = 3.093 \pm 0.001$ by using single Gaussian fitting (Figure 1 right). We measured the total flux density of CO $J = 4 - 3$ by using IMFIT task of CASA on the spectrally integrated flux map with primary beam correction. We checked the total flux density of CO $J = 4 - 3$ by using two components Gaussian fitting on the spectrum data, and found that the result does not significantly change. Following Solomon & Vanden Bout (2005), we estimated the CO $J = 4 - 3$ luminosity of $L'_{\rm CO(4-3)} = (2.3 \pm 0.2) \times 10^9$ K km s^{-1} pc^2 (Table 1).

The CO $J = 4 - 3$ luminosity is used to derive the molecular gas mass with $M_{\rm gas} = r_{41}\alpha_{\rm CO}L'_{\rm CO(4-3)}$, which gives a molecular gas mass of $M_{\rm gas} = (4.4^{+0.9}_{-0.6}) \times 10^9\,M_\odot$ for LAB18.b (Table 1). We adopted luminous submillimetre galaxies (SMGs) median CO $J = 4 - 3$ luminosity to CO $J = 1 - 0$ luminosity ratio of $r_{41} = 0.41 \pm 0.07$ (Bothwell et al. 2013) and starbursts and mergers conversion factor of $\alpha_{\rm CO} = 0.8\,M_\odot$ (K km s^{-1} pc^2)$^{-1}$ (Downes & Solomon 1998) since LAB18.b has a comparable IR luminosity. We note that the molecular gas mass increases by a factor of five given the so-called Galactic conversion factor of $\alpha = 4.36\,M_\odot$ (K km s^{-1} pc^2)$^{-1}$.

The CO $J = 4 - 3$ spectrum for LAB18.b shows double-peaked structure (Figure 1 right) and small spatial offset ($0\farcs4$ or $\sim$3 kpc) between the red and blue components (Figure 1 middle). These suggest that LAB18.b has a rotating disk or a merger, while the beam FWHM is significantly larger than the offset.

3.2 Dust continuum

We detected 2.7 mm and 3 mm dust continuum emission at the position of the LAB18.b (Figure 1 left). We measured the total flux density of both dust continuum emission using IMFIT task of CASA with primary beam correction (Table 1). We derived an infrared (IR) luminosity $L_{\rm IR\,[8-1000\mu m]}$, a dust temperature $T_{\rm d}$ and a dust emissivity index β by fitting a single temperature, optically thin modified black body model to the SPIRE 250 μm (Kato et al. 2016), ALMA Band 7 850 μm (Ao et al. 2017; Matsuda et al. in prep), ALMA Band 3 2.7 mm, and 3 mm dust continuum emission (Figure 2). The SPIRE 250 μm flux density is measured at the position of LAB18.b and applied a source confusion noise for photometry error (Kato et al. 2016). The accuracy of the ALMA Band 7 850 μm absolute flux calibration is evaluated to be within 10%, which is applied for the SED fitting (Figure 2). The best-fit values are $T_{\rm d} = 31.7 \pm 4.1$ K, $\beta = 2.3 \pm 0.2$, and $L_{\rm IR} = (2.7 \pm 1.6) \times 10^{12}\,L_\odot$. These errors show 68% confidence intervals of the χ^2 SED fits to the photometry data. We derived a star-formation rate of SFR$= 269 \pm 158\,M_\odot$ yr^{-1} from the empirical $L_{\rm IR}$-SFR relation in Kennicutt (1998) and Chabrier IMF (Chabrier 2003); SFR$=1.0 \times 10^{-10} L_{\rm IR}$, where the units of SFR and $L_{\rm IR}$ is $M_\odot$ yr^{-1} and $L_\odot$, respectively. The dust mass is also estimated with a relation of $M_{\rm d} = S_{\rm obs}\,D_L^2/(\kappa_{\rm d}(\nu_{\rm rest})\,B_\nu(\nu_{\rm rest}, T_{\rm d})\,(1+z))$; the mass absorption coefficient is $\kappa_{\rm d}(\nu_{\rm rest}) = \kappa_{850}(\nu/\nu_{850})^\beta$, where κ_{850} is assumed to be $\kappa_{850} = 3.2\,{\rm cm^2\,g^{-1}}$ (Demyk et al. 2017). We derived the dust mass of $M_{\rm d} = (4.8 \pm 0.8) \times 10^7\,M_\odot$ using $S_{3\rm mm}$, which indicates gas-to-dust mass ratio of $\delta_{\rm GDR} = 93^{+19}_{-14}$ (Table 1).

We note the SPIRE 250 μm photometry could be overestimated because of source blending with other ALMA 850 μm sources. If the SPIRE 250 μm flux of LAB18.b is proportional to the ALMA 850 μm flux as reported in Ao et al. (2017), the flux decreases by a factor of three and the best-fit results are $T_{\rm d} = 24.1 \pm 1.3$ K, $\beta = 2.6 \pm 0.1$ and $L_{\rm IR} = (1.3 \pm 0.3) \times 10^{12}\,L_\odot$ (Figure 2 open circle). SPIRE source

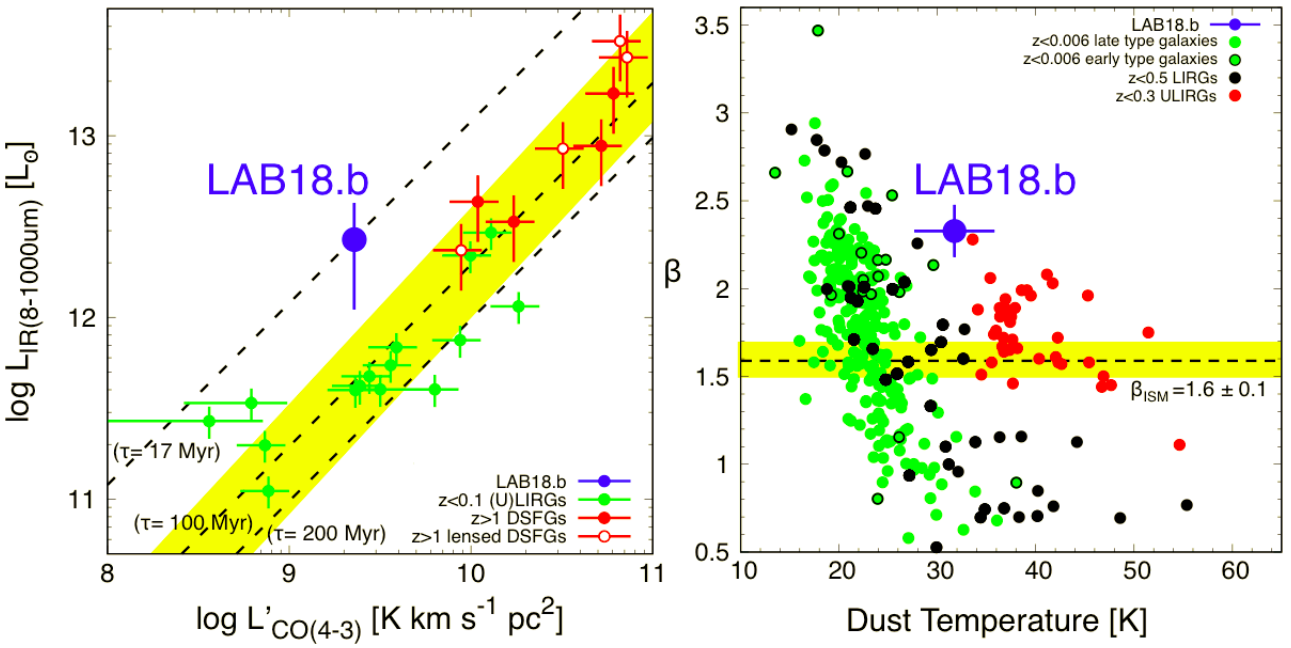

Fig. 3. *(left).* $L_{\rm IR}$ vs. $L'_{\rm CO(4-3)}$ plot. The yellow shaded region is the best-fit relation and its scatter in Greve et al. (2014). The labeled dotted lines show constant molecular gas depletion times. LAB18.b shows one order of magnitude smaller $\tau_{\rm dep}$ than typical DSFGs and (U)LIRGs in Greve et al. (2014). IR luminosities for $z > 1$ lensed DSFGs are corrected for magnification (Greve et al. 2014). *(right).* β vs. $T_{\rm d}$ plot. LAB18.b has a high β compared with the local ULIRGs (red points; Clements et al. 2018) and the Galactic value (yellow shaded region of $\beta = 1.6 \pm 0.1$; Planck Collaboration et al. 2014b). The location of LAB18.b is between local ULIRGs and local gas-poor, early-type galaxies (green points with black circles; Cortese et al. 2014). Black points (LIRGs) and green points (late type galaxies with $L_{\rm IR} = 10^8 - 10^{11}\,L_\odot$) are compiled from Smith et al. (2013) and Cortese et al. (2014), respectively. All data points from literatures use *Hershcel*/SPIRE bands for IR SED fitting with isothermal modified black body model.

confusion does not change our results that LAB18.b has a high β and $L_{\rm IR}$ at a given $L'_{\rm CO(4-3)}$ (Figure 3 left).

4 DISCUSSION AND SUMMARY

Is LAB18.b a typical DSFG at high-redshift? The left panel of Figure 3 shows that LAB18.b has a low $L'_{\rm CO(4-3)}/L_{\rm IR}$ ratio among $z > 1$ DSFGs and $z < 0.1$ (Ultra) Luminous Infrared Galaxies (U)LIRGs in Greve et al. (2014). The labeled dotted lines show constant gas depletion times ($\tau_{\rm dep} = M_{\rm gas}/{\rm SFR}$) derived with $r_{41} = 0.41$, $\alpha = 0.8\,M_\odot$ $({\rm K\,km\,s^{-1}\,pc^2})^{-1}$, and SFR conversion. The derived molecular gas depletion time of LAB18.b is $\tau_{\rm dep} = 17 \pm 10$ Myr, which is one order of magnitude smaller than the typical values of $\tau_{\rm dep} = 100 - 200$ Myr for $z < 0.1$ (U)LIRGs and $z > 1$ DSFGs (Greve et al. 2014). The right panel of Figure 3 shows that LAB18.b is located between local ULIRGs (Clements et al. 2018) and local gas-poor, early-type galaxies (Cortese et al. 2014). These suggest that LAB18.b is not a typical DSFG but in a transition phase from a DSFGs to a gas-poor, early-type galaxy. It would be interesting to test if LABs are associated with DSFGs with short $\tau_{\rm dep}$ and high β by future ALMA observations.

As shown in the right panel of Figure 3, the β of LAB18.b is larger than the typical values of ULIRGs (Clements et al. 2018) and our Galaxy (Planck Collaboration et al. 2014b). What can produce such a high β value? It is known that Îš should be independent of the dust grain size since the observed IR wavelength is much larger than the typical dust grain size in interstellar medium ($0.3\,{\rm nm} \lesssim r \lesssim 0.3\,\mu{\rm m}$; Galliano, Galametz, & Jones 2017). However, a high β can be produced by the chemical composition (e.g., Miyake & Nakagawa 1993). For instance, Demyk et al. (2017) showed that Mg-rich amorphous silicates reproduce $\beta > 2.0$ and a large $\kappa_{850} \sim 3.2\,{\rm cm^2\,g^{-1}}$ compared with the typically assumed values of $\kappa_{850} = 0.4 - 1.5\,{\rm cm^2\,g^{-1}}$ in the diffuse interstellar medium (ISM) in the Galaxy and local galaxies (Dunne et al. 2003). We estimated the $M_{\rm d}$ and $\delta_{\rm GDR}$ for LAB18.b by assuming this $\kappa_{850} = 3.2\,{\rm cm^2\,g^{-1}}$ (§3.2 and Table 1). We note that if we adopt $\kappa_{850} = 1.0\,{\rm cm^2\,g^{-1}}$, the dust mass increases by a factor of three, and results in a small gas-to-dust mass ratio of $\delta_{\rm GDR} \approx 30$, which is much lower than the values in both local (U)LIRGs ($\delta_{\rm GDR} \approx 120$; Wilson et al. 2008) and distant submillimeter galaxies (SMGs) ($\delta_{\rm GDR} \approx 90$; Swinbank et al. 2014). Thus, if LAB18.b has the typical $\delta_{\rm GDR}$ as local (U)LIRGs and SMGs, the large $\kappa_{850} = 3.2\,{\rm cm^2\,g^{-1}}$ expected from the high β is reasonable. We also note that if we estimate the dust mass with $S_{850\,\mu{\rm m}}$, standard $\kappa_{850} = 1.0\,{\rm cm^2\,g^{-1}}$ and $\beta = 2.3$, the dust mass is

still three times smaller than the typical DSFGs estimate (e.g., $S_{850\,\mu m}$, standard $\kappa_{850} = 1.0\,\mathrm{cm^2\,g^{-1}}$ and $\beta = 1.5$). This would support that LAB18.b still ends up with a low dust mass even in a standard κ_{850}, and would support that LAB18.b has low gas mass if the gas-to-dust mass ratio is same as typical DSFGs.

We found that LAB18 has short $\tau_{\rm dep}$ and high β. This suggests that DSFGs in LAB18 are transition phase to evolve gas-poor, early-type galaxies. We argue that ALMA CO and multi-band dust continuum observations can constrain the evolutionary stage of high-redshift galaxies through $\tau_{\rm dep}$ and β. The precise measurement of β can also constrain the chemical composition and κ of dust grains even in the early Universe, which is important to reliable estimate of dust mass.

Acknowledgments

We would like to thank Maciej Koprowski for careful reading our manuscript and for giving useful comments. We thank Ian Smail, Yoichi Tamura, Takaya Nozawa, and Akimasa Kataoka for the useful discussion. We thank L. Cortese, D. J. B. Smith, and T. R. Greve for sharing their data. Y.M, H.U, and Y.T acknowledge JSPS KAKENHI Grant Number 17H04831, 17KK0098, 17K14252 and 16H02166. D.M.A acknowledges the Science and Technology Facilities Council (STFC) through grant ST/P000541/1. Y.A. acknowledges partial support by NSFC grant 1373007. M.H. acknowledges the support of the Swedish Research Council, Vetenskapsrådet and the Swedish National Space Board (SNSB), and is Fellow of the Knut and Alice Wallenberg Foundation. This paper makes use of the following ALMA data: ADS/JAO.ALMA#2016,1.01101.S, ADS/JAO.ALMA#2013.1.00704.S. ALMA is a partnership of ESO (representing its member states), NSF (USA) and NINS (Japan), together with NRC (Canada) and NSC and ASIAA (Taiwan) and KASI (Republic of Korea), in cooperation with the Republic of Chile. The Joint ALMA Observatory is operated by ESO, AUI/NRAO and NAOJ. This work was supported by the ALMA Japan Research Grant of NAOJ Chile Observatory, NAOJ-ALMA-0086.

References

Alexander D. M., et al., 2016, MNRAS, 461, 2944
Ao Y., et al., 2017, ApJ, 850, 178
Bădescu T., Yang Y., Bertoldi F., Zabludoff A., Karim A., Magnelli B., 2017, ApJ, 845, 172
Barger A. J., Cowie L. L., & Wold I. G. B., 2012, ApJ, 749, 106
Boselli A., et al., 2012, A&A, 540, A54
Bothwell M. S., et al., 2013, MNRAS, 429, 3047
Cai Z., et al., 2017, ApJ, 837, 71
Caminha G. B., et al., 2016, A&A, 595, A100
Chabrier G., 2003, PASP, 115, 763
Chapman S. C., Lewis G. F., Scott D., Richards E., Borys C., Steidel C. C., Adelberger K. L., & Shapley A. E., 2001, ApJ, 548, L17
Chapman S. C., Scott D., Windhorst R. A., Frayer D. T., Borys C., Lewis G. F., & Ivison R. J., 2004, ApJ, 606, 85
Clements D. L., et al., 2018, MNRAS, 475, 2097
Cortese L., et al., 2014, MNRAS, 440, 942
Demyk K., et al., 2017, A&A, 600, A123
Dey A., et al., 2005, ApJ, 629, 654
Downes D., Solomon P. M., 1998, ApJ, 507, 615
Dunne L., Eales S., Edmunds M., Ivison R., Alexander P., Clements D. L., 2000, MNRAS, 315, 115
Dunne L., Eales S., Ivison R., Morgan H., Edmunds M., 2003, Natur, 424, 285
Galliano F., Galametz M., Jones A. P., 2017, arXiv, arXiv:1711.07434
Geach J. E., et al., 2005, MNRAS, 363, 1398
Geach J. E., et al., 2009, ApJ, 700, 1
Geach J. E., et al., 2014, ApJ, 793, 22
Geach J. E., et al., 2016, ApJ, 832, 37
Ginolfi M., et al., 2017, MNRAS, 468, 3468
Greve T. R., et al., 2005, MNRAS, 359, 1165
Greve T. R., et al., 2014, ApJ, 794, 142
Hildebrand R. H., 1983, QJRAS, 24, 267
Hine, N. K., et al., 2016, MNRAS, 460, 4075
Hodge J. A., Carilli C. L., Walter F., Daddi E., Riechers D., 2013, ApJ, 776, 22
Jones A. P., 2002, EAS, 4, 37
Kato Y., et al., 2016, MNRAS, 460, 3861
Kennicutt R. C., Jr., 1998, ARA&A, 36, 189
Kubo M., Yamada T., Ichikawa T., Kajisawa M., Matsuda Y., Tanaka I., Umehata H., 2016, MNRAS, 455, 3333
Lehmer B. D., et al., 2009, MNRAS, 400, 299
Matsuda Y., et al., 2004, AJ, 128, 569
Matsuda Y., et al., 2009, MNRAS, 400, L66
Matsuda Y., et al., 2011, MNRAS, 410, L13
McMullin J. P., Waters B., Schiebel D., Young W., Golap K., 2007, ASPC, 376, 127
Meny C., Gromov V., Boudet N., Bernard J.-P., Paradis D., Nayral C., 2007, A&A, 468, 171
Miyake K., Nakagawa Y., 1993, Icar, 106, 20
Planck Collaboration, et al., 2014a, A&A, 571, A16
Planck Collaboration, et al., 2014b, A&A, 571, A11
Prescott M. K. M., Kashikawa N., Dey A., Matsuda Y., 2008, ApJ, 678, L77
Prescott M. K. M., et al., 2012, ApJ, 752, 86
Smith D. J. B., et al., 2013, MNRAS, 436, 2435
Solomon P. M., Vanden Bout P. A., 2005, ARA&A, 43, 677
Steidel C. C., Adelberger K. L., Dickinson M., Giavalisco M., Pettini M., Kellogg M., 1998, ApJ, 492, 428
Steidel C. C., Adelberger K. L., Shapley A. E., Pettini M., Dickinson M., & Giavalisco M., 2000, ApJ, 532, 170
Swinbank A. M., et al., 2014, MNRAS, 438, 1267
Tacconi L. J., et al., 2018, ApJ, 853, 179
Tadaki K.-i., et al., 2017, ApJ, 841, L25
Tamura Y., et al., 2013, MNRAS, 430, 2768
Umehata H., et al., 2017a, ApJ, 835, 98
Umehata H., et al., 2017b, ApJ, 834, L16
Umehata H., et al., 2018, arXiv, arXiv:1804.08842
Valentino F., et al., 2016, ApJ, 829, 53
Wilson C. D., et al., 2008, ApJS, 178, 189-224
Yang Y., Walter F., Decarli R., Bertoldi F., Weiss A., Dey A., Prescott M. K. M., Bădescu T., 2014, ApJ, 784, 171